In Situ X-ray Absorption of Co/Mn/TiO₂ Catalysts for Fischer−Tropsch Synthesis

Fernando Morales,[†] Frank M. F. de Groot,[†] Pieter Glatzel,[†] Evgueni Kleimenov,[‡] Hendrik Bluhm,[‡,§] Michael Hävecker,[‡] Axel Knop-Gericke,[‡] and Bert M. Weckhuysen*,[†]

Department of Inorganic Chemistry and Catalysis, Utrecht University, Debye Institute, Sorbonnelaan 16, 3584 CA Utrecht, The Netherlands, and Fritz-Haber-Institut der MPG, Faradayweg 4-6, D-14195 Berlin, Germany

Received: May 26, 2004; In Final Form: August 5, 2004

The reduction behavior of Co/TiO₂ and Co/Mn/TiO₂ catalysts for Fischer−Tropsch synthesis has been investigated by soft X-ray absorption spectroscopy (XAS). In situ XAS measurements of the L₂,₃ edges of Co and Mn have been carried out during reduction treatments of the samples in H₂ at a pressure of 2 mbar and at temperatures up to 425 °C. The changes of Co and Mn 3d valences and the symmetries throughout the reduction have been determined by comparison with theoretical calculations based on the charge transfer multiplet code. Furthermore, bulk Co₃O₄ has been reduced under the same conditions to evaluate the effect of TiO₂ as a support on the reducibility of Co oxides. The average Co valence at the various temperatures has been determined from a linear combination of the reference spectra. It was found that the unsupported Co₃O₄ was easily reduced to Co⁰ at 425 °C, whereas the Co₃O₄ supported on TiO₂ catalysts was only reduced to a mixture of CoO and Co⁰, even after 12 h reduction at 425 °C. The presence of Mn further retards the reduction of the supported Co₃O₄ particles. The Mnᴵᴵᴵ ions were easily reduced to MnO at temperatures lower than 300 °C, and they remained in this oxidation state even after further temperature increase. In addition, catalytic tests in the Fischer−Tropsch synthesis reaction at a pressure of 1 bar indicate that the selectivity of these catalysts might be related to the extent of Co reduced after the activation treatment (i.e., the reduction with H₂).

Introduction

The transformation process from syngas to hydrocarbons, Fischer−Tropsch synthesis (FTS), is gaining in importance due to the need for high purity fuels, which can be obtained from feedstocks other than crude oil (i.e., natural gas, charcoal, or biomass). These materials are converted into syngas by partial oxidation or steam reforming processes.[1] Supported Co catalysts are claimed to be the most effective in achieving higher chain growth probability values (α) and turnover rates compared to other metal based catalysts. This makes them the catalysts of choice for FTS.[2,3] Reducibility of supported-cobalt particles strongly depends on the support used[4−6] and on the preparation method.[7,8] For supports without a strong interaction with cobalt, such as silica, highly reducible cobalt oxide clusters are normally formed.[9,10] TiO₂-supported catalysts have been shown to have a strong metal−support interaction,[6] which makes the cobalt species difficult to be reduced, most likely due to a strong Co−O interaction with the support or the formation of other stable compounds (e.g., cobalt titanate (CoTiO₃)) that are reduced only at very high temperatures. The formation of the cobalt titanate species has been reported before,[6,11] and it is thought to occur during the reduction from Co₃O₄ crystallites to CoO. During the reduction process, Coᴵᴵ can diffuse into the support lattice, leading to the formation of these compounds. The use of other metals in small amounts (i.e., promoter elements) has been

investigated over recent decades with the aim of enhancing the catalytic performances of Co-based catalysts. The use of manganese compounds as promoters for the hydrogenation of carbon monoxide has been previously investigated. It was shown that manganese promoters can increase the olefin selectivity of Co-based catalysts in the FTS reaction and under certain circumstances can enhance their activity and shift the distribution of products toward larger chain hydrocarbons.[12,13] However, the exact role of such promoters and their influence on the state of cobalt particles throughout the FTS reaction remains unclear.

The use of in situ techniques for the characterization of surfaces in heterogeneous catalysts is becoming an important tool to investigate these materials under reaction conditions. Photons in the range 100−1000 eV are suitable probes for the electronic structure of reacting surfaces. Their interaction with solid matter leads to photoabsorption processes, which can be detected by the electrons created typically from a surface depth of several nanometers, making the low energy XAS technique surface sensitive. In recent years, it has become possible to perform XAS measurements at pressure ranges of 1−10 mbar,[14] which allows the carrying out of in situ treatments of the samples (e.g., calcinations and reductions), providing useful information about the surface composition of the catalysts under conditions that are closer to the actual operating conditions. The L₂,₃ XAS spectral shapes of the 3d transition metal oxides can be simulated accurately using the charge transfer multiplet code.[15−17] These calculations take into account the local symmetry and hybridization. In general, they reproduce the L₂,₃ XAS very well, thereby yielding information on the local symmetry (octahedral vs tetrahedral, high spin vs low spin) including the crystal field values and symmetry dependent covalence.[18]

---

* To whom correspondence should be addressed. E-mail: b.m.weckhuysen@chem.uu.nl.

[†] Utrecht University.

[‡] Fritz-Haber-Institut der MPG.

[§] Present address: Chemical Sciences Division, Lawrence Berkeley National Laboratory, One Cyclotron Road, Berkeley, California 94720.

In our study, in situ XAS measurements during reduction treatments were carried out with two catalysts (Co/TiO_2 and $Co/Mn/TiO_2$) and with a bulk Co_3O_4. With this work, we aim to investigate the valences and symmetry of states for Mn and Co at the different temperatures during the reduction and, moreover, to evaluate the influence of TiO_2 support on the reducibility of the Co oxides due to the so-called metal−support interaction. Bazin et al.[19] have performed similar experiments before on Co/SiO_2 catalysts. In their study, they carried out the XAS measurements in a UHV chamber, which was coupled to another chamber for the sample treatments. However, this fact can significantly affect the cobalt sites. For instance, the changes in the pressure/gas environment before and during the measurements can influence the average valence state of the cobalt sites. In situ XAS studies on other catalyst systems reveal that significant changes in the average valence can occur within oxide materials.[20]

Experimental Section

1. Materials and Catalyst Preparation. Two TiO_2-supported catalysts were synthesized using the homogeneous deposition precipitation (HDP) technique to load the Co and incipient wetness impregnation (IWI) to load the Mn. Commercial Degusa P25 titania (surface area of 45 m^2/g and pore volume of 0.27 cm^3/g) was used as the support material. The powder titania was suspended in an aqueous solution containing cobalt nitrate, and the pH was slowly increased by urea decomposition at 90 °C under continuous stirring for 18 h. After drying at 110 °C overnight, the material was sieved and a portion was calcined in air at 400 °C for 4 h with a heating rate of 5 °C/min, obtaining the Co/TiO_2 catalyst. For the preparation of the Mn-promoted catalyst, the other portion was impregnated with an aqueous solution of manganese nitrate followed by the same calcination procedure described above, obtaining the $Co/Mn/TiO_2$ catalyst. The Co and Mn loadings of both calcined catalysts were determined by X-ray fluorescence analysis (XRF). The loadings obtained were 7.5 wt % Co and 2 wt % Mn, respectively. The high purity Co_3O_4 material was obtained from Merck, and the reference compounds MnO, Mn_2O_3, and MnO_2 were obtained from Aldrich.

2. X-ray Diffraction. The bulk phase composition of both catalysts was investigated after calcination by X-ray diffraction (XRD). Powder XRD measurements were performed using an ENRAF-NONIUS XRD system with a curved position sensitive INEL detector and applying a Co $K\alpha_1$ radiation source ($\lambda = 1.788\,97$ Å). In addition to the reflections of the TiO_2 support, only the diffraction peaks corresponded to the Co_3O_4 phase were detected. The mean Co_3O_4 particle sizes were determined from the line broadening of the diffraction line situated at 43.3°, applying the Scherrer equation. The particle sizes obtained were ∼15 and ∼13 nm for the Co/TiO_2 and $Co/Mn/TiO_2$ catalyst, respectively.

3. In Situ Soft X-ray Absorption Spectroscopy. The soft X-ray absorption spectra of the manganese $L_{2,3}$ edge (635−660 eV), the cobalt $L_{2,3}$ edge (770−800 eV), and the titanium $L_{2,3}$ edge (450−470 eV) were measured at beamline U56/2 PGM-2 at BESSY (Berlin). The spectral resolution of the monochromator was ∼0.2 eV. The instrumentation for in situ XAS and XPS measurements is described elsewhere.[21] A stainless steel in situ cell was used in which the powdered samples were fixed in a sample holder. The X-ray absorption spectral shape was measured with the ionized gas conversion total electron yield, which has a probing depth of approximately 4 nm.
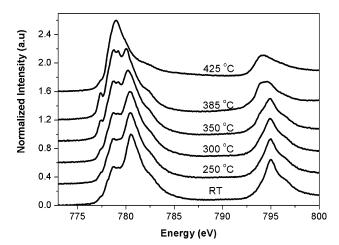

Figure 1. Co $L_{2,3}$ edges for bulk Co_3O_4 during reduction from RT to 425 °C. All spectra have been normalized from zero to one.

The experiments were carried out during reduction treatments under a dynamic atmosphere (i.e., flowing in H_2). The samples were inserted into the chamber, which was subsequently pumped down to vacuum. After approximately 5 min, the chamber was brought under pure hydrogen (100 mL/min) using a mass flow controller. A gas mixing system regulated the flow and the total pressure at the sample position, which was 2 mbar during the experiments. After optimization of the signal by tuning the slit size and the spot of the incoming beam, the temperature was increased from RT to 425 °C with a ramp of 5 °C/min. The ramp was temporarily stopped at 300, 350, and 425 °C to measure both the Co and the Mn L edges. The bulk Co_3O_4 was measured at 385 °C, in addition to the same temperatures used to measure the catalysts. In addition, the catalysts were held under H_2 atmosphere at 425 °C for 12 h to evaluate further changes in the spectra with reduction time. The electron yield was measured by applying a voltage of 27 V on the first aperture, which is electrically isolated from the cell.

4. Temperature Programmed Reduction Experiments. The reduction behavior of the supported metal oxides was studied at a pressure of 1 bar by temperature programmed reduction (TPR) using a "Thermo Electron TPDRO 1100" piece of equipment. The experiments were performed in a tubular quartz reactor. After loading the sample, the reactor was flushed with Ar at 120 °C for 1 h and then cooled to RT in flowing Ar. Subsequently, the gas flow was adjusted to 5% H_2/Ar and the temperature was raised at the rate of 10 °C/min from RT to 600 °C. The content of H_2 in the outflowing gas was monitored with a thermoconductivity detector throughout the reduction treatment.

5. Catalytic Testing. The FTS reaction was carried out using a glass plug flow reactor in which the calcined catalysts were diluted in SiC. Before starting the reaction, the samples were in situ activated in 20 mL/min flow of H_2 at 350 °C for 2 h. The reaction was carried out at a pressure of 1 bar, a temperature of 220 °C, and a H_2/CO ratio of 2 in the syngas composition. The gas hourly space velocity (GHSV) was adjusted to obtain CO conversions of ∼3%. The reaction temperature was measured with a thermocouple inserted in the catalyst bed. The hydrocarbon products' composition was analyzed on-line using a Varian CP-3800 gas chromatograph equipped with a fused silica column of 50 m length and a flame ionization detector.

Results

1. Co 2p XAS of Co_3O_4. Figure 1 shows the Co $L_{2,3}$ edge spectra of the bulk Co_3O_4 measured during the reduction

In Situ X-ray Absorption of Co/Mn/TiO₂ Catalysts

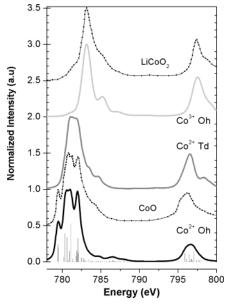*J. Phys. Chem. B, Vol. 108, No. 41, 2004* **16203**

Figure 2. Co L$_{2,3}$ edges of the reference compounds LiCoO$_2$ and CoO, together with charge transfer multiplet (CTM) calculations of the cobalt sites. From bottom to top, the spectra are respectively, the CTM calculation of Co^{II} (O$_h$), the CoO spectrum, the CTM calculation of Co^{II} (T$_d$), the CTM calculation of Co^{III} (O$_h$), and the LiCoO$_2$ spectrum. The CoO and LiCoO$_2$ spectra, reproduced from de Groot et al.[24] and de Groot,[25] are reproduced by the calculations shown below them.

treatment from RT up to 425 °C. It can be observed that the spectrum shape changes by increasing the temperature. At the same time, the maximum energy peak shifts to lower energies. These spectral changes are due to a shift from higher to lower cobalt valence and variations in the symmetry of the cobalt atomic states upon reduction. Comparison of the experimental spectra (Figure 2) with the theoretical simulations led us to a better understanding of these spectrum shapes. The spectrum measured at RT corresponds to a mixture of Co^{II} and Co^{III} oxidation states (ratio of 1/2) characteristic of Co$_3$O$_4$. Co$_3$O$_4$ has a spinel type structure where the oxygen atoms are arranged in a fcc structure, and Co^{II} (T$_d$) and Co^{III} (O$_h$) cations are located in tetrahedral and octahedral coordination, respectively.[22] As soon as the temperature increases, the shape of the spectra becomes more purely Co^{II} since Co$_3$O$_4$ is reduced to CoO. In the CoO, the Co^{II} cations are octahedral coordinated by the oxygen atoms. When the temperature reaches 385 °C, the measured spectrum corresponds to pure CoO, as shown in the comparison with a reference sample (Figure 2). This confirms the complete shift of cobalt to Co^{II} (O$_h$) at 385 °C. The consecutive reduction of CoO to Co^0 easily occurs at 425 °C, at which point the pure Co^0 spectrum is obtained. This spectrum consists of a single peak at the L$_3$ edge, characteristic of Co metal.[24]

Figure 2 shows the Co 2p X-ray absorption spectra of CoO and LiCoO$_2$, together with the charge transfer multiplet (CTM)
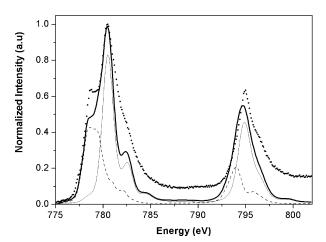

Figure 3. CTM calculations of octahedral Co^{III} (thin solid) and tetrahedral Co^{II} (dashed). These spectra have been added with a 2:1 ratio (thick solid) to simulate the experimental Co$_3$O$_4$ spectrum (points).

calculations of the cobalt sites. CoO contains octahedral Co^{II} sites, and LiCoO$_2$ contains octahedral Co^{III} sites. The charge transfer parameters of the Co^{II} (O$_h$) sites have been optimized to CoO, following the literature data.[25] These parameters are collected in Table 1. The CTM spectrum of Co^{II} (O$_h$) includes the calculated energy intensity multiplet spectrum. These stick spectra have been broadened with the 2p lifetime broadening and an experimental broadening that is assumed to be a Gaussian. The Lorentzian broadening is 0.4 eV for the L$_3$ edge and 0.8 eV for the L$_2$ edge. The Gaussian broadening is 0.4 eV. Similarly, the Co^{II} (O$_h$) site has been optimized to LiCoO$_2$. In the case of LiCoO$_2$ the agreement is not exactly correct, and the experimental spectrum has a clear shoulder at 781 eV and a less structured shoulder/peak at 785 eV.

Figure 3 shows the comparison of the CTM calculations of octahedral Co^{III} and tetrahedral Co^{II} with Co$_3$O$_4$. These simulations confirm that Co$_3$O$_4$ indeed consists of octahedral low spin (^{1}A$_1$) Co^{III} and tetrahedral high spin (^{4}A$_2$) Co^{II} sites. Comparison to the LiCoO$_2$ spectrum in Figure 2 showed that LiCoO$_2$ also contains low spin (^{1}A$_1$) Co^{III} sites. The addition of twice the spectrum of Co^{III} plus one of the spectrum of Co^{II} is used to simulate the experimental spectrum of Co$_3$O$_4$. Some discrepancies are visible in the simulation, but these are mostly due to the imperfect simulation of the low spin (^{1}A$_1$) Co^{III} sites, as it was also the case for the LiCoO$_2$ spectrum in Figure 2. Exactly like the LiCoO$_2$ spectrum, Co$_3$O$_4$ also has extra intensity at 781 eV and a less pronounced structure at 785 eV. Taking this into account, the simulations confirm that Co$_3$O$_4$ consists of octahedral low spin (^{1}A$_1$) Co^{III} and tetrahedral high spin (^{4}A$_2$) Co^{II} sites.

Figure 4 shows the comparison of the CoO reference spectrum with the experimental spectrum of Co$_3$O$_4$ at 385 °C. Because the L$_3$ edge shows much more structure than the L$_2$ edge, we only show the L$_3$ edge region. The good agreement confirms

TABLE 1: Charge Transfer Parameters Used for the Calculations of Theoretical Spectra^a

parameter	CoO	LiCoO$_2$	Co^{II} in Co$_3$O$_4$
site symmetry	Co^{II} (O$_h$)	Co^{III} (O$_h$)	Co^{II} (T$_d$)
electronic symmetry	high spin: ^{4}T$_1$, split by spin orbit to E	low spin: ^{1}A$_1$	high spin: ^{4}A$_2$,
ionic crystal field [10Dq]^b	0.6	1.9	−0.3
charge transfer energy [Δ]^c	3.0	4.5	7.0
hopping e$_g$-electrons^b [t$_e$]	2.0	2.0	1.0
hopping t$_{2g}$-electrons^b [t$_t$]	1.0	1.0	2.0

^{a} All values are given in eV. ^{b} Hopping adds a "covalent contribution" to the overall crystal field (or ligand field) strength of ∼0.3 eV for the values used. ^{c} Core hole potential Q is assumed to be 2.0 eV higher than the 3d3d repulsion energy U, which implies that the final state charge transfer energy $\Delta' = \Delta - 2.0$ eV.[25,26]
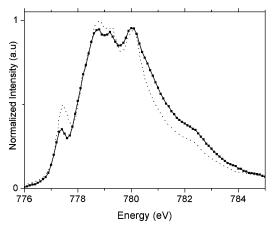
Figure 4. Comparison of the room temperature CoO reference spectrum (dotted) with the experimental spectrum of Co_3O_4 at 385 °C (solid, with solid squares).

Figure 5. Co $L_{2,3}$ edges measured for the Co/Mn/TiO$_2$ catalyst during reduction. At RT, the spectrum corresponds mainly to Co_3O_4, which is reduced to CoO at 350 °C. After 12 h of reduction at 425 °C, the spectrum corresponds to CoO + Co^0.

that at 385 °C, Co_3O_4 is indeed fully reduced to CoO. There are some small differences visible. The shoulder at 777 eV is smaller in the reduced Co_3O_4, and the peaks at ∼779−780 eV are slightly lower in the reduced Co_3O_4. A reason for these small differences can be found in the difference in measurement temperature between the CoO reference (RT) and the Co_3O_4 sample (385 °C). It is known that the X-ray absorption spectra of CoO have a temperature dependence due to the population of excited states.[24,25] In addition, it is likely that in the reduced Co_3O_4 the crystallinity of the CoO is not perfect and there will be some variation in site symmetry, oxygen vacancies, etc. These variations will make the resulting spectrum slightly different and can explain the small differences observed.

In conclusion, it is found from the reference compounds and from the CTM calculations that Co_3O_4 is a mixture of octahedral ($^1A_1$) Co^{III} and tetrahedral ($^4A_2$) Co^{II} sites. During reduction, the Co^{III} is reduced to octahedral ($^4T_1$) Co^{II}; in addition, the tetrahedral ($^4A_2$) Co^{II} sites are modified into octahedral ($^4T_1$) Co^{II} sites in CoO. All spectra at intermediate temperatures can be considered as a linear combination of the spectra of Co_3O_4 and CoO.

2. Co 2p XAS of the (Mn)/Co/TiO$_2$ Catalysts. The Co $L_{2,3}$ edges of the catalysts were measured at 25, 300, 350, and 425 °C, in addition to another measurement performed after 12 h at 425 °C. It was found that the reduction behavior was rather similar in both catalysts, but significantly different from the bulk cobalt oxide discussed above. As an example, we show the spectra of the Co/Mn/TiO$_2$ catalyst in Figure 5. At RT, the spectra of both catalysts correspond to (mainly) Co_3O_4. The reduction of Co_3O_4 to CoO is achieved at lower temperatures than in the bulk Co_3O_4. This might be due to the lower cobalt content in the catalyst, which results in less time needed to achieve the complete reduction to CoO. In none of the catalysts did the CoO compounds significantly reduce to Co^0 at 425 °C. Instead, the spectra consist mainly of CoO with only a small amount of Co^0. These results indicate that CoO supported on TiO$_2$ is difficult to reduce to Co^0 at the conditions used in this work (i.e., 2 mbar of H$_2$ at 425 °C).

To quantify the changes of the Co valence throughout the reduction, linear combinations of the spectra of the pure Co compounds were used to calculate the Co average valence at each temperature. For these calculations, the experimental spectra of bulk cobalt measured at RT, 385, and 425 °C were used as the spectra of the pure Co_3O_4, CoO, and Co^0 compounds, respectively. Hence, the change of cobalt valence with temperature could be followed and compared in both the catalysts and
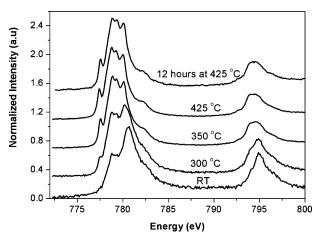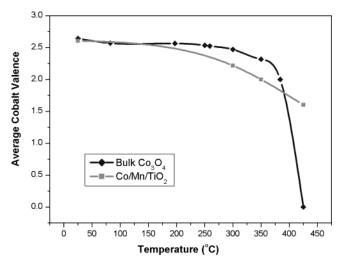

Figure 6. Comparison of the average Co valence for the bulk Co_3O_4 and the Co/Mn/TiO$_2$ catalyst during the reduction treatment.

the bulk cobalt during the reduction. Figure 6 shows a comparison of the bulk Co_3O_4 with the Co/Mn/TiO$_2$ catalyst. It can be observed that unsupported Co_3O_4 is reduced to Co^0 at 425 °C, in contrast with the TiO$_2$-supported cobalt catalyst that is only partly reduced under the same conditions. Furthermore, some differences in the amount of cobalt metal were found between both catalysts after the full reduction. The surface Co compositions were calculated for both catalysts after 12 h of reduction at 425 °C. The compositions obtained were 39% Co^0 and 61% CoO for the Co/TiO$_2$ catalyst and 25% Co^0 and 75% CoO for the Co/Mn/TiO$_2$ catalyst. Hence, the presence of Mn in the catalyst was found to decrease the amount of Co^0 obtained after H$_2$ reduction at a pressure of 2 mbar.

3. Mn 2p XAS of the Mn/Co/TiO$_2$ Catalysts. The three manganese reference compounds were measured at RT to obtain the spectra of pure Mn^{IV}, Mn^{III}, and Mn^{II}. Figure 7 shows the 2p X-ray absorption spectra of the MnO, Mn$_2$O$_3$, and MnO$_2$ references. The Mn spectra can again be simulated using CTM calculations, as discussed previously.[25] We will now use these reference compounds in the analysis of the Mn spectra of the catalyst.

The Mn $L_{2,3}$ edges of the Co/Mn/TiO$_2$ catalyst were measured at the same conditions as Co, at RT and during the reduction at 300, 350, and 425 °C. Changes in the shape of the spectra were found between RT and 300 °C, whereas the spectra did not
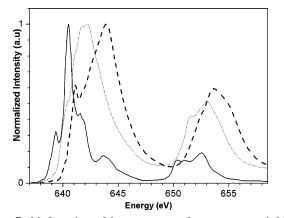
Figure 7. Mn L$_{2,3}$ edges of the manganese reference compounds MnO (solid), Mn$_2$O$_3$ (dots), and MnO$_2$ (dashed).
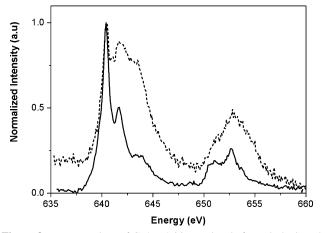

Figure 8. Mn L$_{2,3}$ edges of Co/Mn/TiO$_2$ catalyst before (dashed) and after (solid) the reduction treatment.

change more by raising the temperature above 300 °C. For this reason, we only show the spectra before and after the treatment (Figure 8). By comparing the measured spectra of the catalyst with the reference compounds, it can be concluded that the Mn contained in the calcined catalyst consists of a mixture of Mn^{II} and Mn^{III}, with possibly some admixture of Mn^{IV}. The spectral shape indicates that Mn^{III} is the predominant Mn species, which could be in the form of Mn$_2$O$_3$, although it is also plausible that some mixed oxides such as Co$_2$MnO$_4$ and Mn$_2$CoO$_4$ are present, as reported in the literature.[26] However, the spectral quality does not allow for an accurate quantification of the amount of each compound. Upon reduction, the Mn present in the catalysts is already fully reduced to MnO at 300 °C, and no other variations are found in the spectra recorded at higher temperatures. The absence of the peak at 639 eV in the experimental spectra of the catalysts is due to a smaller value of the crystal field, which is influenced by defects in the crystal structure. These results indicate a high stability of MnO at these reduction conditions and are in agreement with other work where MnO was also found to be the main compound in supported manganese oxide catalysts after reduction.[27]

4. Temperature Programmed Reduction. Figure 9 shows the TPR profiles obtained for both catalysts. The reduction of the Co/TiO$_2$ catalyst results in two main peaks with maxima at 280 and 455 °C. We attribute these two H$_2$-consumption peaks to the reduction steps from Co$_3$O$_4$ to CoO and from CoO to Co^0. The areas of the two peaks are in agreement with the stoichiometry of both reduction steps, which is in the ratio of 1/3. Moreover, the second reduction step shows two different maxima (350 and 455 °C), and this suggests a different extent
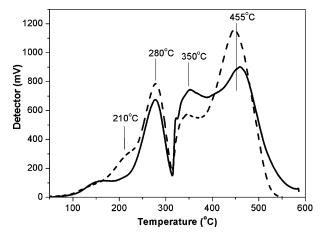

Figure 9. TPR profiles of Co/TiO$_2$ (solid) and Co/Mn/TiO$_2$ (dashed) catalysts.

TABLE 2: FTS Catalytic Performances

sample code	Co-time yield^a	% CH$_4$ selec.	% C$_{5+}$ selec.	α values^b	butane/butene ratio
Co/TiO$_2$	2.35	31.6	28.0	0.54	0.34
Co/Mn/TiO$_2$	2.50	24.9	34.8	0.58	0.22

^{a} Co-time yield: 10^{-5} mol CO (g Co)$^{-1}$ s^{-1}. ^{b} As calculated from the slope between C$_3$ and C$_7$ in the ASF distribution plot, according to the equation log W_n/n = log(ln^2 α) + n log α, where W_n is the weight fraction of the products with n carbon number.

of Co−support interaction present in the catalyst. The Co/Mn/TiO$_2$ catalyst shows a similar TPR profile, although the maximum temperature peak of the second reduction step is somewhat more pronounced. Therefore, this experiment indicates a decrease of the cobalt reducibility in the Co/Mn/TiO$_2$ catalyst with respect to the Co/TiO$_2$ catalyst. In addition, the small peak appearing at ∼210 °C for the Co/Mn/TiO$_2$ catalyst is attributed to the reduction of the Mn oxides.

5. Catalytic Testing. Catalytic performances of the catalysts were compared at pseudo-steady-state conditions after a 40 h FTS reaction. The activities were calculated as the % CO converted into hydrocarbons without taking into account other side reactions (i.e., CO$_2$ formation). The paraffin/olefin ratios were calculated using the butane and butene yields. Table 2 gathers the resulting catalytic performances for both catalysts after 40 h of reaction. The Co/Mn/TiO$_2$ catalyst gave a slightly higher Co-time yield than the Co/TiO$_2$ catalyst, although this small difference is within the measurement error. On the other hand, the presence of Mn in the Co/Mn/TiO$_2$ catalyst resulted in a suppression of the methane make and enhanced the selectivity toward high weight hydrocarbons (lower % CH$_4$ and higher % C$_{5+}$). In addition, a small increase of the chain growth probability (α) was found. This shift in the product's mass distribution for the Mn-promoted catalyst was accompanied by an increase of the olefinic product yield.

Discussion

It has been shown that the use of soft X-ray absorption spectroscopy as a tool for studying the composition of catalyst surfaces can be of great interest for determining the oxidation state of 3d transition metals during the activation of the catalysts. Moreover, the fact that most catalytic reactions take place at the surface of the metal particles makes this technique very attractive for studying catalytic systems, since the information obtained corresponds to a depth of a few nanometers into the metal surface, not to the bulk. Nevertheless, the low pressure

conditions (2 mbar) required to perform these measurements are still too far from the actual operating conditions (1 bar or higher). Therefore, the information obtained with the XAS technique cannot be directly correlated with that from other characterization techniques.

With the current experiments, we intended to investigate the surface composition of the cobalt and manganese contained in two FTS catalysts. The XAS measurements allowed us to calculate the valences of both transition metals, which play a role during FTS reaction (i.e., after the activation treatment). It turned out that the support oxide has a strong influence on the reduction behavior of the cobalt oxides, since CoO could not be reduced to Co^0 in any of the supported catalysts, whereas a bulk Co_3O_4 sample could be fully reduced to metallic Co. This should be due to the existence of a strong cobalt−support interaction, which makes it difficult for the CoO reduction to occur in the presence of TiO_2 support. This fact suggests that the active sites of FTS catalysts may consist of a mixture of Co^0 and Co^{II} and that their composition depends on the pretreatment performed before FTS reaction and on the extent of metal−support interaction present in the catalyst. We note that the present result does not allow us to judge exactly what kind of mixture between Co^0 and Co^{II} exists. Possible options are a physical mixture of Co and CoO, as well as the existence of another phase (for example, a suboxide and/or a changed microstructure). Here, we note that the CoO nanoparticles are quite small ($\sim$10−20 nm), and in case of a mixed metal−oxide particle there will be a significant percentage of cobalt atoms that will feel neither a potential as pure Co (nanosize) metal nor a potential of pure CoO. The only conclusion we would like to draw is the measured ratio of Co to CoO, which best explains the observed spectral shape.

The XAS measurements allowed measuring of the amount of Co^0, and the surface of the cobalt particles contained in the three samples after the reduction treatments can be ordered, from most to least metallic, as follows: Co_3O_4 > Co/TiO_2 > $Co/Mn/TiO_2$. From this calculation, we can see that both TiO_2 and Mn have an effect on the extent of Co^0 at the surface of the Co particles. The presence of Mn in the catalyst prevents the CoO reducibility to some extent at 2 mbar conditions. In addition, a similar trend is found with the reduction experiments at 1 bar. This decrease of the Co reducibility is reflected in the catalytic performances mainly by an increase in olefin yield and a decrease in CH_4 formation. These results suggest that a more oxidic composition of the cobalt surface favors the chance to terminate the hydrocarbon growth by β-hydrogen abstraction, leading to an increase of the α-olefin content in the product composition. However, this suppression in the hydrogenation rate found for the $Co/Mn/TiO_2$ catalysts might be merely related to the presence of MnO interacting with the Co particles, rather than the more oxidic Co surface resulting upon the decrease of the Co reducibility. We note that even though the TPR experiments provide a trend similar to the XAS measurements concerning the Co reducibility in both catalysts, it is uncertain what their Co surface composition is under FTS conditions, since the Co sites may suffer structural and compositional changes during FTS.[28] Hence, the changes in selectivity may be also accounted to the presence of MnO. Similar effects on Mn-promoted catalysts have been observed before by other groups.[12,13] Therein, they found a higher selectivity toward light olefins and a lower CH_4 production in the FTS upon Mn addition to Co-based catalysts, although no characterization was conducted to explain the reasons for these selectivity changes. Furthermore, the enhancement of the C_{5+} selectivity found in this work may be due to the modified catalyst surface resulted upon the Mn addition, which restrains the secondary hydrogenation of olefins with respect to the Co/TiO_2 catalyst. The chain growth probabilities are thought to be clearly influenced by the rate of α-olefin reattachment on the Co surface and subsequent growth.[29] Therefore, the restriction of the secondary hydrogenation of olefins leads to a more effective chain growth in the promoted catalyst. Other work has also reported changes in the α as a function of paraffin/olefin ratios.[30]

Conclusions

TiO_2 influences the reduction behavior of Co_3O_4 particles by decreasing the extent of reduced cobalt present in the catalysts after reduction. The final cobalt composition of the TiO_2-supported catalysts was mainly CoO and some amount of Co^0, whereas bulk Co_3O_4 could be reduced to pure Co^0 after the same treatment. These results point toward the existence of a strong Co−TiO_2 (metal−support) interaction, which affects the composition of the reduced catalysts. The Mn contained in the $Co/Mn/TiO_2$ catalyst after calcination was found to be present as a mixture of Mn^{II}, Mn^{III}, and Mn^{IV}, and as soon as the catalyst was reduced at 300 °C, only MnO was measured. Furthermore, these Mn compounds had an extra effect on the Co reducibility of this catalyst, since the final amount of Co^0 was significantly lower than in the Co/TiO_2 catalyst. This decrease of the Co reducibility resulted in an increase of the C_{5+} yield and a higher olefin selectivity without any loss in FTS activity.

References and Notes

(1) Rostrup-Nielsen, J. R. *Catal. Today* **2002**, *71*, 243.
(2) Iglesia, E. *Appl. Catal., A* **1997**, *161*, 59.
(3) Schulz, H. *Appl. Catal., A* **1999**, *186*, 3.
(4) Bartholomew, C. H.; Reuel, R. C. *Ind. Eng. Chem.* **1985**, *24*, 56.
(5) Riva, R.; Miessner, H.; Vitali, R.; Del Piero, G. *Appl. Catal., A* **1999**, *196*, 111.
(6) Vob, M.; Borgmann, D.; Wedler. *J. Catal.* **2002**, *212*, 10.
(7) Jacobs, G.; Das, T. K.; Zhang, Y.; Li, J.; Racoillet, G.; Davis, B. H. *Appl. Catal., A* **2002**, *233*, 263.
(8) Kraum, M.; Baerns, M. *Appl. Catal., A* **1999**, *186*, 189.
(9) Coulter, K. E.; Sault, A. G. *J. Catal.* **1995**, *154*, 56.
(10) Ernst, B.; Libs, S.; Chaumette, P.; Kiennemann, A. *Appl. Catal., A* **1999**, *186*, 145.
(11) Brik, Y.; Kacimi, M.; Ziyad, M.; Bonzon-Verduraz, F. *J. Catal.* **2001**, *202*, 118.
(12) Barrault, J. *Stud. Surf. Sci. Catal.* **1982**, *11*, 225.
(13) Van der Riet, M.; Copperthwaite, R. G.; Hutchings, G. J. *J. Chem. Soc., Faraday Trans. 1* **1987**, *83*, 2963.
(14) Knop-Gericke, A.; Havecker, M.; Schedel-Niedrig, T.; Schlogl, R. *Top. Catal.* **2000**, *10*, 187.
(15) de Groot, F. M. F.; Fuggle, J. C.; Thole, B. T.; Sawatzky, G. A. *Phys. Rev. B.* **1990**, *42*, 5459.
(16) de Groot, F. M. F. *J. Elect. Spectrosc. Relat. Phenom.* **1994**, *67*, 529.
(17) de Groot, F. M. F. *Chem. Rev.* **2001**, *101*, 1779.
(18) Wasinger, E. C.; de Groot, F. M. F.; Hedman, K. O.; Hodgson, K. O.; Solomon, E. I. *J. Am. Chem. Soc.* **2003**, *125*, 12894.

In Situ X-ray Absorption of Co/Mn/TiO₂ Catalysts

J. Phys. Chem. B, Vol. 108, No. 41, 2004 **16207**

(19) Bazin, D.; Kovacs, I.; Guczi, L.; Parent, P.; Laffon, C.; de Groot, F. M. F.; Ducreux, O. *J. Catal.* **2000**, *189*, 456.

(20) Heijboer, W. M.; Battiston, A. A.; Knop-Gericke, A.; Havecker, M.; Mayer, R.; Bluhm, H.; Schlogl, R.; Weckhuysen, B. M.; Koningsberger, D. C.; de Groot, F. M. F. *J. Phys. Chem. B.* **2003**, *107*, 13069.

(21) Ogletree, D. F.; Bluhm, H.; Lebedev, G.; Fadley, C. S.; Hussain, Z.; Salmeron, M. *Rev. Sci. Instrum.* **2002**, *73*, 3872.

(22) Kim, K. J.; Park, Y. R. *Solid State Commun.* **2003**, *127*, 25.

(23) Chen, C. T.; Idzerda, Y.; Lin, H. J.; Smith, N. V.; Meigs, G.; Chaban, E.; Ho, G. H.; Pellegrin, E.; Sette, F. *Phys. Rev. Lett.* **1995**, *75*, 152.

(24) de Groot, F. M. F.; Abbate, M.; Van Elp, J.; Sawatzky, G. A.; Ma, Y. J.; Chen, C. T.; Sette, F. *J. Phys.: Condens. Matter* **1993**, *5*, 2277.

(25) de Groot, F. M. F. Ph.D. Thesis, 1991.

(26) Cuse, K.; Rapp, H. *J. Anal. Chem.* **1993**, *346*, 84.

(27) Boot, L. A.; Kerkhoffs, M. H. J. V.; Van der linder, B. T.; Dillen, A. J. V.; Geus, J. W.; Van Buren, F. R. *Appl. Catal., A* **1996**, *137*, 69.

(28) Schulz, H.; Nie, Z.; Ousmanov, F. *Catal. Today* **2002**, *71*, 351.

(29) Iglesia, E.; Soled, S. L.; Fiato, R. A.; Via, G. H. *J. Catal.* **1993**, *143*, 345.

(30) Kuipers, E. W.; Vinkenburg, I. H.; Oosterbeek, H. *J. Catal.* **1994**, *152*, 137.